



Original Article

# Retrorsine Cooperates with Gut Microbiota to Promote Hepatic Sinusoidal Obstruction Syndrome by Disrupting the Gut Barrier

Li Xiao<sup>1,2#</sup>, Lilin Hu<sup>1#</sup>, Huikuan Chu<sup>1#</sup>, Liuying Chen<sup>1</sup>, Jingjing Yan<sup>1</sup>, Weijun Wang<sup>1</sup>,  
Xiaoqian Yang<sup>1</sup>, Qingjing Zhu<sup>3</sup>, Fan Du<sup>1</sup>, Yuhu Song<sup>1</sup>, Peng Chen<sup>4</sup>, Xiaohua Hou and Ling Yang<sup>1\*</sup>

<sup>1</sup>Division of Gastroenterology, Union Hospital, Tongji Medical College, Huazhong University of Science and Technology, Wuhan, Hubei, China; <sup>2</sup>Department of Gastroenterology, Henan Provincial People's Hospital, People's Hospital of Zhengzhou University, School of Clinical Medicine, Henan University, Zhengzhou, Henan, China; <sup>3</sup>Wuhan Jinyintan Hospital, Wuhan, Hubei, China; <sup>4</sup>Department of Pathophysiology, School of Basic Medical Science, Southern Medical University, Guangzhou, Guangdong, China

Received: 7 September 2021 | Revised: 20 December 2021 | Accepted: 18 January 2022 | Published: 11 March 2022

## Abstract

**Background and Aims:** Hepatic sinusoidal obstruction syndrome (HSOS) is a life-threatening syndrome, and a cause is exposure to pyrrolizidine alkaloid (PA)-containing products. It is well-established that retrorsine (RTS), a representative Pas, insults hepatic sinusoidal endothelial cells and ensues congestion of hepatic sinusoids. However, little known about the impact of Pas on gut microbiota and intestinal barrier and inflammation in HSOS. **Methods:** Mice were gavaged with or without nonabsorbable antibiotics (ABX), followed by a single dose of RTS. The gut microbiota was examined by 16S rDNA sequencing. **Results:** ABX pretreatment significantly reversed RTS-induced liver damage. RTS altered gut microbiota composition, increasing Gram-negative bacteria and resulting in a sharp elevation of circulating lipopolysaccharides (LPS) in HSOS mice. Gut decontamination with ABX alleviated RTS-induced intestine inflammation, protected against disruption of the intestinal epithelial barrier and gut vascular barrier (GVB), and suppressed hepatic LPS-NF- $\kappa$ B pathway activation in RTS-induced HSOS. Importantly, the LPS level was positively correlated with MELD score in patients with HSOS. Elevated LPS in patients

with HSOS confirmed that Gram-negative bacteria were involved in the pathogenesis of HSOS. **Conclusions:** RTS, a PA, cooperated with gut dysbiosis to cause intestinal inflammation and gut barrier compromise that increased transport of gut-derived LPS into the liver through the portal vein, which contributed to the pathology of HSOS. Modulating the gut microbiota, protecting the intestinal barrier, and suppressing intestinal inflammation with prebiotics or antibiotics might be a useful pharmacologic intervention in HSOS.

**Citation of this article:** Xiao L, Hu L, Chu H, Chen L, Yan J, Wang W, et al. Retrorsine Cooperates with Gut Microbiota to Promote Hepatic Sinusoidal Obstruction Syndrome by Disrupting the Gut Barrier. J Clin Transl Hepatol 2022;10(6):1086–1098. doi: 10.14218/JCTH.2021.00398.

## Introduction

Pyrrolizidine alkaloid (PA)-induced hepatic sinusoidal obstruction syndrome (HSOS), is a potentially life-threatening complication clinically characterized by hepatomegaly, ascites, and hyperjaundice because of injured hepatic sinusoidal endothelial cells and congestion of hepatic sinusoids.<sup>1</sup> In China, a common etiology of HSOS is exposure to PA-containing products such as Tusanqi (*Gynura segetum*), a traditional Chinese herbal medicine.<sup>2</sup> Pas are constitutively expressed in herbal plants worldwide, frequently in plant families consumed by humans.<sup>3</sup> It is currently believed that Pas are bioactivated as electrophilic pyrrolic metabolites to initiate hepatotoxicity.<sup>4</sup> The active metabolite combines with glutathione (GSH) to form glutathione conjugates that result in exhaustion of hepatic GSH, or couple with DNA and proteins to form pyrrole-adducts, which are proposed to be the main mechanism for PA-induced HSOS.<sup>5</sup> Retrorsine (RTS), is a representative PA that exists in nature and has been extensively investigated. However, the mortality of clinical HSOS induced by Pas varies widely, from 3% to 60% because of the lack of effective medical treatment.<sup>6</sup> The variability suggests that in addition to PA-induced HSOS,

**Keywords:** Retrorsine; Pyrrolizidine alkaloids; Hepatic sinusoidal obstruction syndrome; Gut microbiota; Drug-induced liver injury.

**Abbreviations:** ABX, nonabsorbable antibiotics; ALT, alanine aminotransferase; AST, alanine aminotransferase; ELISA, enzyme-linked immunosorbent assay; FD70, 70 kD fluorescein isothiocyanate-dextran; GAPDH, glyceraldehyde-3-phosphate dehydrogenase; GVB, gut vascular barrier; H&E, hematoxylin and eosin; HSOS, hepatic sinusoidal obstruction syndrome; IKK $\beta$ , inhibitor of nuclear-factor kappa-B kinase subunit beta; LDA, Linear discriminant analysis; LefSe, linear discriminant analysis effect size; LPS, lipopolysaccharides; MELD, model for end-stage liver disease; NF- $\kappa$ B, nuclear-factor-kappa B; NMDS, non-metric multidimensional scaling; p, phosphorylated; PA, pyrrolizidine alkaloid; PCA, principal components analysis; PcoA, principal co-ordinates analysis; PCR, polymerase chain reaction; PV1, plasmalemma vesicle-associated protein-1; RTS, retrorsine; TLR4, Toll-like receptor 4.

#Contributed equally to this work.

\*Correspondence to: Ling Yang, Division of Gastroenterology, Union Hospital, Tongji Medical College, Huazhong University of Science and Technology, 1277 Jiefang Avenue, Wuhan, Hubei 430022, China. ORCID: <https://orcid.org/0000-0002-0751-5600>. Tel: +86-27-85726678, +86-13971178791, Fax: +86-27-85726678, E-mail: [hepayang@163.com](mailto:hepayang@163.com), [mailto:yanglinguh@hust.edu.cn](mailto:mailto:yanglinguh@hust.edu.cn)

other pathophysiological mechanisms may be involved.

The gut-liver-axis is involved in the pathophysiology of many liver diseases.<sup>7</sup> involves reciprocal interactions of the intestine, microbiota, and the liver. The balance of the microbial communities is essential for maintaining the homeostasis of the gut-liver axis, and in turn, the liver shapes the gut microbial communities.<sup>8</sup> Rapidly accumulating evidence has demonstrated that the gut microbiota has an important role in the pathogenesis of various liver diseases via the gut-liver axis. For example, the gut microbiota mediates diurnal variation of acetaminophen-induced acute liver injury in mice.<sup>9</sup> Moreover, intestinal bacteria translocate into the liver to promote hepatic inflammation during CCl<sub>4</sub>-induced fibrosis.<sup>10</sup> Dysbiosis and gut inflammation can exacerbate liver inflammatory responses by overloaded exposure to bacterial components and harmful metabolites of the microbiome.<sup>11</sup> Dysbiosis also affects bile acid metabolism, and composition of the gut microbiota, and intestine and liver immune function.<sup>12,13</sup> Healthy intestinal epithelial and vascular barriers are the foundation of the crosstalk between the liver and intestine.<sup>14</sup> As the critical mechanical barrier, the intestinal epithelial barrier formed with tight junctions that prevent foreign substances from moving out of the gut into the lamina propria.<sup>15</sup> The gut vascular barrier (GVB) is the last defensive barrier to prevent harmful microbial components and metabolites from entering the portal circulation. If a macromolecule or a microorganism crosses the epithelial barrier, it is localized in the lamina propria, only if the GVB is also compromised.<sup>16</sup> Importantly, dysbiosis can further insult the intestinal barrier and exaggerate intestinal inflammation.<sup>17,18</sup> These findings imply that gut dysbiosis and enhanced intestinal permeability and inflammation are important in the pathology contributing to the progress of liver diseases. However, in the context of HSOS, it has not been investigated if there exists a change of microbial composition, increased intestinal inflammation, and intestinal permeability. This study investigated whether RTS caused HSOS by triggering perturbation of gut microbiota, impairment of the gut barrier, and activation of intestinal inflammation, and whether those factors, likely act in parallel to promote the pathogenesis of HSOS.

## Methods

### Animals

All animal care and experimental procedures were approved by the Animal Experimentation Ethics Committee of Tongji college, Huazhong University of Science and Technology (ethical approval number S2597). Animals received humane care and all procedures were performed following the guidelines published by the National Academy of Sciences and the National Institutes of Health. Male specific pathogen-free C57BL/6 mice 8 weeks of age and weighing 20–22 g (Beijing HFK Bio-Technology Co., Ltd.) were used. They were housed in a specific pathogen-free facility at Tongji college, Huazhong University of Science and Technology at 22±2°C, relative humidity 60–70% and a 12/12 h light/dark cycle.

Mice were gavaged with 100 mg/kg RTS (Sigma-Aldrich, St. Louis, MO, USA) or an equal volume of saline vehicle. RTS was added to distilled water at 10 mg/mL and titrated to pH 2.5 with 1N HCl to completely dissolve the solid. The solution was then neutralized (pH 7.0) with 1N NaOH.<sup>19</sup> The working solution was used immediately after preparation. For antibiotic treatment, mice were given intragastric vancomycin (100 mg/kg), neomycin sulfate (200 mg/kg), metronidazole (200 mg/kg), and ampicillin (200 mg/kg) once daily for 5 days.<sup>9</sup> Mice were anesthetized with 50 mg/kg,

intraperitoneal pentobarbital sodium, and sacrificed 24 h after RTS administration.

### Fecal colony culture

To evaluate the effect of ABX treatment on the numbers of fecal colonies, mice were treated with ABX for seven consecutive days. Feces of four wild-type C57/BL6 mice were collected before ABX treatment and at 1, 2, 3, 4, 5, 6, and 7 days of ABX treatment. Feces were weighed, added to sterile PBS (10 µl PBS/mg feces), and 100 µL of the suspension was evenly spread onto solid TSB medium by glass beads. Colonies were counted with the naked eye after incubation at 37°C 24 h. The colony forming units (CFU)/g feces were calculated.

### Liver function assays

Liver function was assayed by plasma alanine aminotransferase (ALT) activity and plasma alanine aminotransferase (AST) with commercial Assay Kits (Jiancheng Bioengineering Institute, Nanjing, China) following the manufacturer's instructions.

### Histological and immunohistochemical staining

Sections of formalin-fixed tissue were stained with hematoxylin and eosin (H&E) and masson for visualizing histological features. To quantify inflammatory cell infiltration liver sections were incubated with CD11b (ab133357; Abcam, Cambridge, UK) and F4/80 (ab111101; Abcam) primary antibodies at 4°C overnight, followed by incubation with an HRP-conjugated secondary antibody (ANT020; Antgen, Wuhan, China).

### Enzyme-linked immunosorbent assay (ELISA)

Serum proinflammatory cytokines tumor necrosis factor alpha (TNF-α) and interleukin (IL)-6 were measured by commercial ELISA kits (NewBioscience, Shenzhen, China) following the manufacturer's protocols.

### Analysis of fecal microbiota composition by 16S rDNA sequencing

Total genome DNA was extracted from stool samples using Soil DNA kits (MoBio, Carlsbad, CA, USA) following the manufacturer's protocols. DNA concentration was monitored by Qubit3.0 Fluorometer (Life Technologies, Carlsbad, CA, USA) for further analysis. The V3 and V4 hypervariable regions of 16S rDNA were selected for generating amplicons and for taxonomy analysis. Indexed adapters were added to the ends of the 16S rDNA amplicons to generate indexed libraries ready for downstream next generation sequencing on an Illumina MiSeq. DNA library concentrations were read with a Qubit3.0 Fluorometer. Quantified to 10 nM, DNA libraries were multiplexed and loaded on an Illumina MiSeq instrument following the manufacturer's instructions (Illumina, San Diego, CA, USA). Sequencing was performed using PE250/300 paired-end. Image analysis and base calling were conducted with MiSeq Control Software embedded in the MiSeq instrument. After quality assessment, operational taxonomic units (OTUs) were clustered and taxonomic annotation was performed in VSEARCH (version 1.9.6). The

sequence similarity was set at 97%.<sup>20</sup> The abundance of species at the phylum, class, order, family, genus, and species levels of classification was determined with QIIME version 1.9.1.<sup>21</sup> Mothur version v.1.39 was used to generate alpha diversity indices (Chao1 index, Shannon index, and Simpson index).<sup>22</sup> Principal component analysis (PCA), principal co-ordinate analysis (PcoA), and non-metric multidimensional scaling (NMDS) were used to visualize beta diversity. Analysis of similarity (ANOSIM) was conducted to assess the statistical significance of differences in bacterial composition among the different samples. To study the differences in the abundance of microbial community species in different groups of samples, the between-group difference in species abundance was tested by Metastats.<sup>23</sup> Linear discriminant analysis (LDA) effect size (LefSe) was performed to analyze the differences of the species among groups and branching tree diagrams showed the hierarchy of evolution between-group differences of microbial community structure and species.<sup>23</sup> Differences were considered statistically significant at  $p < 0.05$ .

### Cell culture

Caco-2 human intestinal epithelial cells and HCT116 human colorectal cancer cells were cultured in Gibco PRIM 1640 and DMEM media, respectively, supplemented with 10% fetal bovine serum (FBS), penicillin, and streptomycin. Cells were maintained in a 5% CO<sub>2</sub> incubator at 37°C and were routinely tested to exclude mycoplasma contamination. During the study, Caco2 cells were stimulated with RTS (600 µmol/L) and LPS (10 µg/mL) and HCT116 cells were stimulated with RTS (600 µmol/L) and LPS (5 µg/mL) for 24h. Controls were treated with the same amount of vehicle.

### GVB permeability measurement

To test the GVB permeability, mice were given 1 mg/ml FITC-dextran 70 kDa (FD70; Sigma-Aldrich Corp., St. Louis, MO, USA) into the ileal loop under anesthesia. Blood specimens were collected by heart puncture after 1 h. The fluorescence of FD70 in serum was detected using a fluorescence microplate reader (BioTek Instruments, Winooski, VT, USA). The dye intensity of FD70 in liver and spleen was observed in optimum cutting temperature (OCT)-frozen sections by confocal fluorescence microscopy (TCS SP8X; Leica, Wetzlar, Germany).

### Serum lipopolysaccharide (LPS) assay

Mouse portal vein serum and human plasma were collected and preserved in endotoxin-free tubes at -80°C. LPS was assayed with mouse and human LPS ELISA kits (Cusabio, Wuhan, China) following the manufacturer's protocols. Optical density was measured at 450 nm with a microplate reader.

### Real-time quantitative PCR (qPCR)

Total RNA was extracted with Trizol Reagent (TaKaRa, Dalian, China) and reverse-transcribed into cDNA using PrimeScript RT Master Mix kits (RR036A; TaKaRa) following the manufacturer's instructions. qPCR was performed with gene-specific primers and SYBR Premix Ex Taq (RR420A; TaKaRa) on a Roche LightCycler 480 System. Relative mRNA

levels were normalized against *GAPDH*. The primer pairs are listed in Supplementary Table 1.

### Western blotting

Total protein was extracted in RIPA lysis buffer, followed by ultrasonication, and centrifugation at 12,000 rpm for 10 min at 4°C. Protein concentration in the supernatant was determined with a bicinchoninic acid (BCA) assay (23225; Thermo Fisher Scientific, Waltham, MA, USA). Proteins were separated on 10% SDS-PAGE gels and then transferred to PVDF membranes (IPVH00010; Merck Millipore, Darmstadt, Germany) in ice water. After blocking in 5% BSA/TBST for 1 h at room temperature, membranes were incubated with primary antibodies overnight at 4°C: ZO-1, 1:500 (ab96587; Abcam); occludin, 1:1,000 (331594; ThermoFisher Scientific); PV1, 1:500 (ab27853; Abcam); inhibitor of nuclear-factor kappa-B kinase subunit beta (IKKβ), 1:1,000 (8943; Cell Signaling Technology, Danvers, MA, USA); p-IKKβ, 1:1,000 (2697; Cell Signaling Technology); p65, 1:1,000 (3022; Cell Signaling Technology); p-p65, 1:1,000 (3031; Cell Signaling Technology); GAPDH, 1:3,000 (ANT012; Antgene); Actin, 1:2,000 (ANT010; Antgene), followed by incubation with corresponding secondary antibody (1:3,000; Antgene) for 1 h at room temperature. GAPDH was the loading control. The protein bands were observed and quantified by Image Lab Software (Bio-Rad, Hercules, CA, USA) following the manufacturer's instructions.

### Human blood samples

Assays involving clinical blood samples were approved by the Review Board of the Affiliated Union Hospital of Tongji Medical College, Huazhong University of Science and Technology (approval number: S1027). The assays followed the ethical principles of the Declaration of Helsinki. Informed consent forms were signed by all participants. The study cohort provided 12 blood specimens.

### Statistical analysis

Statistical analysis was performed with SPSS Statistics version 22.0 (IBM Corp., Armonk, NY, USA). Results were reported as means ± standard errors of the mean. Between-group comparisons were performed with two-tailed Student's *t*-tests. One-way analysis of variance was used to assess statistical significance in multiple-group comparisons. The threshold for statistical significance was set at  $p < 0.05$ . GraphPad Prism (version 7) was used to construct graphs.

## Results

### Gut microbiota participates in RTS-induced HSOS

To explore the characteristic pattern of PA-induced HSOS model, hepatotoxicity induced by RTS was monitored in mice at 24 h after a single oral administration of 40, 70, 100, or 140 mg/kg. When mice were given 100 mg/kg, liver injury was more severe and manifested with typical HSOS histological features, such as the dilation of sinusoids and destruction of central veins, Serum ALT and AST activity levels were also significantly elevated (Supplementary Fig. 1A, B). To explore the contribution of the intestinal microbiota to RTS-induced liver injury, we first established an intestinal decontamination model by oral administration mixed

nonabsorbable antibiotics (ABX). We found that almost no colonies grew in fecal cultures following continuous ABX treatment for 5 days compared with the vehicle group (Supplementary Fig. 2), which indicated nearly complete suppression of the gut microbiota. Then we subjected mice to ABX administration continuously for 5 days followed by a single oral dose of RTS to observe the role of gut microbiota in HSOS model. Without ABX pretreatment to decontaminate the gut, RTS caused significant hepatomegaly, liver congestion, hepatic sinus expansion (Fig. 1A–C). Necrotic areas in the pericentral zone and serum ALT and AST elevation were seen 24 h after RTS administration (Fig. 1D, E). Masson staining showed fibrous tissue around small veins in the livers of HSOS mice (Supplementary Fig. 3). ABX pretreatment greatly alleviated the RTS-induced increases of ALT and AST. Histological evaluation found with much less liver necrosis and fibrous tissue formation than the group without ABX pretreatment. ABX pretreatment also markedly attenuated the expression of genes associated with hepatic inflammation, including *Mcp1*, *Il1 $\beta$* , *Il6*, *Tnfa*, *Cxcl1*, *Cxcl10*, and *Ccl4* in mice with RTS-induced HSOS (Fig. 1F, G). ABX pretreatment also reduced the number of infiltrating Kupffer cells/macrophages, which are the major source of inflammatory cytokine production in response to liver damage in RTS-induced HSOS mice, that were positive for CD11b- and F4/80 (Fig. 1H). ABX pretreatment significantly suppressed the expression of genes associated with endothelial dysfunction, including *ET1*, *iNOS*, *Cd44*, *Vcam1*, *Icam1*, and *PAI1*, which was induced by RTS in HSOS mice (Fig. 1I). The data indicate that intestinal decontamination significantly alleviated HSOS caused by RTS, and that gut microbiota participated in the pathogenesis of HSOS induced by RTS.

### **RTS modifies gut microbiota composition in HSOS mice**

To further detect the composition of gut microbiota in RTS-induced HSOS, we performed 16S rDNA sequencing. We first assessed the microbiota colony composition by  $\alpha$ -diversity indices by the Chao1, Shannon, and Simpson methods. As shown, RTS group had a remarkable reduction of the bacterial biodiversity, with lower Chao1, Shannon, and Simpson indices compared with those of vehicle group. ABX pretreatment led to a more significant reduction in the bacterial biodiversity and cleared almost all bacteria (Fig. 2A–C and Supplementary Fig 2). ANOSIM demonstrated that the difference between vehicle and RTS group was significantly greater than the differences within the group (Fig. 2D).  $\beta$ -diversity determined by UniFrac analysis was used to evaluate differences of community biodiversity among groups by NMDS diagrams, PCA, and PcoA. The  $\beta$ -diversity indices revealed a marked compositional shift in RTS group relative to the vehicle group, with distinctive microbial community structures in the RTS and vehicle groups (Fig. 2E–G). Taxon-based analysis disclosed that RTS led to a distinct shift at the phylum (Fig. 2H), family (Fig. 2J), and genus (Fig. 2K) levels. RTS-induced HSOS mice had a significant decrease in the abundance of phylum Firmicutes but an increase in the abundance of phylum Bacteroidetes relative to the vehicle, which reflects the shift of the integral gut microbial composition (Fig. 2H). The relative abundance of Gram-negative bacteria producing plentiful LPS was significantly elevated in RTS vs. vehicle (Fig. 2I). The Firmicutes families Ruminococcaceae and Lachnospiraceae were significantly decreased in the RTS relative to vehicle mice. However, the Bacteroidetes family Bacteroidaceae and the Proteobacteria family Enterobacteriaceae were significantly increased in the HSOS mice (Fig. 2J). We

observed decreases of families Lachnospiraceae and Ruminococcaceae, and genus *Lactobacillus*, but increases in the genera *Bacteroides*, *Escherichia/Shigella*, *Alloprevotella*, and family Prevotellaceae in HSOS mice (Fig. 2K). LefSe was performed to identify significant differences in microbiota composition between the RTS and control groups. A differential cladogram demonstrated that phylum Firmicutes was dominant in vehicle group versus phylum Bacteroidetes in the RTS group (Fig. 2L). LefSe identified 57 taxonomic clades with an LDA score  $>3$  and  $\alpha < 0.05$  that were significantly altered in relative abundance between RTS and vehicle. The genera *Bacteroides*, *Escherichia/Shigella*, *Prevotellaceae\_UCG\_001*, *Bilophila*, *Alloprevotella*, *Lachnospirillum*, and *Parabacteroides* were abundant in RTS group. *Ruminococcaceae\_UCG\_014/009*, *Lachnospiraceae\_NK4A136\_group*, *Gordonibacter*, *Lactobacillus* were concentrated in vehicle group (Fig. 2M). Considering that the sharply increased abundance of Bacteroidetes as the largest component of Gram-negative bacteria could result in the production of LPS, we measured the LPS level in portal vein serum. RTS mice had significantly higher serum LPS levels than the vehicle mice, and decontaminating the flora with ABX attenuated the elevation of LPS in HSOS mice (Fig. 2N). All of the above findings reveal that RTS administration alone remarkably altered the microbial community structure in HSOS mice, especially elevating the abundance of Gram-negative bacteria and leading to a significant increase of LPS.

### **RTS cooperates with gut microbiota to induce intestinal inflammation**

We observed that RTS caused intestinal mucosal injury and mild inflammatory cell infiltration in tissue stained with hematoxylin and eosin (Fig. 3A). As illustrated, the mRNA levels of innate immunity components (*Cd14*, *Tlr4*, *Tlr9*) were also slightly upregulated by RTS administration and reversed by ABX pretreatment (Fig. 3B). RTS induced a low-grade inflammatory response with increased levels of inflammatory cytokine mRNA, including *Il-6*, *Ccl2*, *Ccl4*, *Cxcl2*, and *Icam1*, relative to those of given vehicle or treated with ABX+RTS. Similarly, ABX administration significantly decreased the extent of upregulation of the expression inflammatory cytokine RNAs (Fig. 3C). As shown in Fig. 2, the LPS level was significantly elevated, so we focused specifically on the LPS-activated nuclear-factor kappa B (NF- $\kappa$ B) pathway in the intestine. Phosphorylation of NF- $\kappa$ B signaling proteins, IKK $\beta$  and p65 were significantly augmented compared with those of the control group, and pretreatment with ABX significantly inhibited the activation of NF- $\kappa$ B signaling (Fig. 3D). The results indicate that RTS cooperated with gut microbiota to upregulate the expression of NF- $\kappa$ B pathway and that intestinal decontamination with ABX restrained RTS-induced activation of the NF- $\kappa$ B pathway in HSOS mice. As LPS is the main byproduct of the Gram-negative bacteria in the gut, we performed cell experiments to confirm whether RTS combined with LPS induced intestinal inflammation. HCT116 human colon carcinoma cells were treated with RTS (600  $\mu$ M) and LPS (5  $\mu$ g/mL) for 24 h to mimic the intestinal environment of HSOS. Consistent with the *in vivo* observations, we found that costimulation with RTS and LPS significantly increased the expression of the inflammation-related genes *IL-6*, *TNFA*, *CCL2*, *CCL4* and *CXCL2* (Fig. 3E), as well as the activation of NF- $\kappa$ B pathway (Fig. 3F, G). Taken together, the results show that RTS enhanced intestinal inflammatory responses to LPS when gut microbiota were present, that the inflammatory response was decreased by pretreatment with ABX, and that RTS cooperated with gut microbiota and LPS to promote intestinal inflammation.

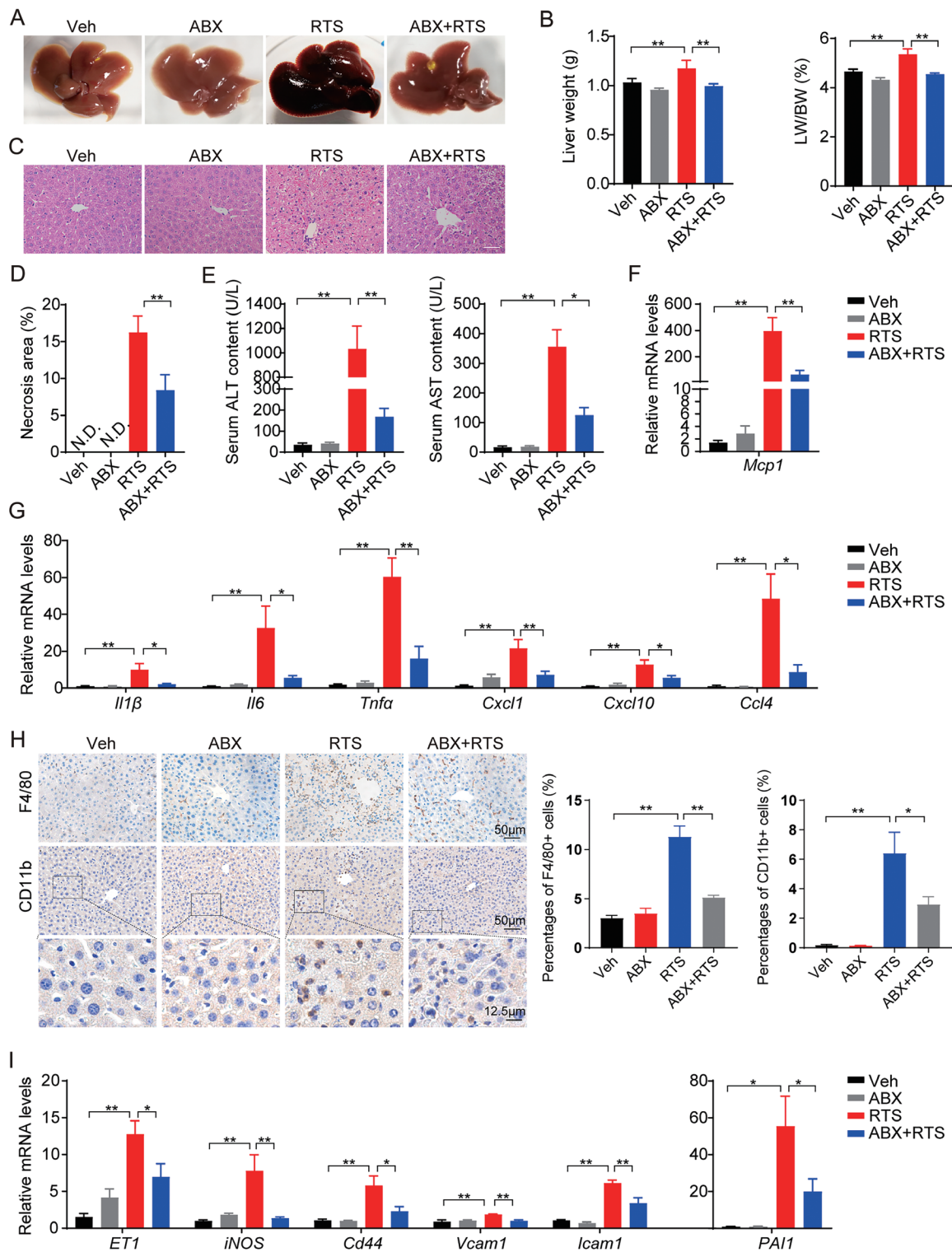


**Fig. 1. Gut microbiota participates in RTS-induced HSOS in male C57BL/6 mice treated with RTS for 24 h with or without ABX pretreatment.** (A) Representative gross liver appearance. (B) Liver weight (left) and the ratio of the liver weight and body weight (right),  $n=8$ . (C) Hepatic hematoxylin and eosin staining, scale bar, 100  $\mu$ m. (D) Necrotic area,  $n=6$ . (E) Serum ALT and AST. (F, G) mRNA expression of pro-inflammatory factors (*Mcp1*, *Il1 $\beta$* , *Il6*, *Tnfa*, *Cxcl1*, *Cxcl10*, and *Ccl4*) in the liver,  $n=6$ . (H) Representative images of inflammatory cell infiltration staining in liver sections (left) and percentages of F4/80+ cells and CD11b+ cells (right). (I) mRNA levels of endothelial dysfunction related genes (*ET1*, *iNOS*, *Cd44*, *Vcam1*, *Icam1*, and *PAI1*),  $n=6$ . The results are means  $\pm$  standard error of the mean. \* $p<0.05$ , \*\* $p<0.01$  (analysis of variance). ABX, nonabsorbable antibiotics; ALT, alanine aminotransferase; AST, alanine aminotransferase; LW/BW, ratio of liver weight and body weight; ND, not detectable; RTS, retrorsine; Veh, vehicle.

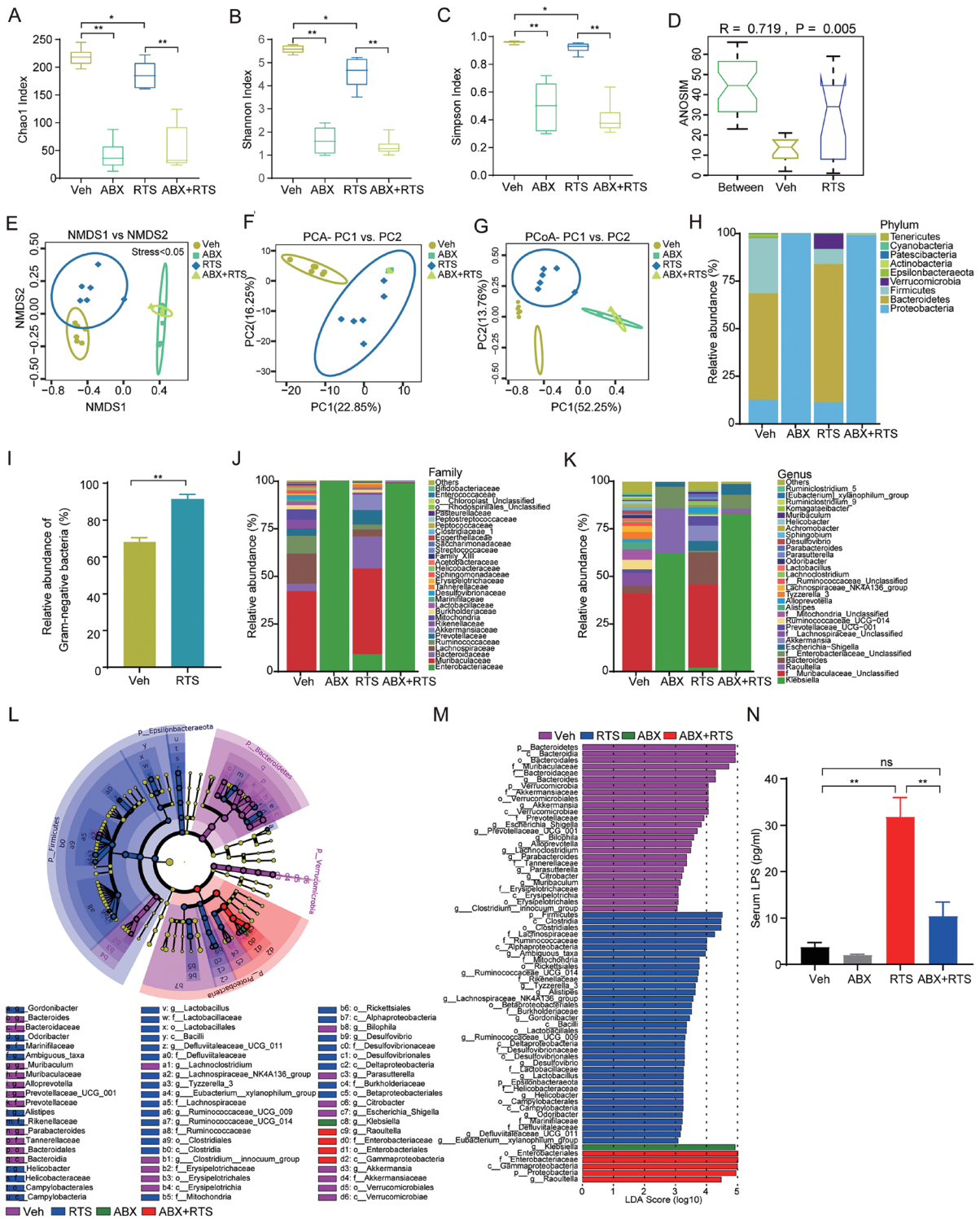


**Fig. 2. RTS modifies gut microbiota composition in HSOS mice.** (A-C) Comparison of  $\alpha$ -diversity among groups. Three indices were used to represent the  $\alpha$ -diversity by the (A) Chao1 index, (B) Shannon index, and (C) Simpson index. Data are means $\pm$ 95% confidence interval. \* $p$ <0.05, \*\* $p$ <0.01; paired t-test. (D) Analysis of similarity (ANOSIM) of indicating significant differences between the groups when  $R$ >0 and  $p$ <0.05. (E) Nonmetric multidimensional scaling (NMSD) showing the difference in bacterial communities. (F) Principal component analysis (PCA) and (G) Principle coordinate analysis (PCoA) plot of similarities among the different groups. The top relative abundances of bacteria at the phylum (H), family (J) and genus (K) levels in cecal content samples among the study groups. (I) Relative abundance of Gram-negative bacteria. (L) Cladogram showing the most differentially abundant taxa identified by linear discriminant analysis (LEfSe). (M) Linear discriminant analysis (LDA) value distribution histogram showing species with an LDA >3. For A–M,  $n$ =6 per group. (N) Serum LPS level ( $n$ =8 per group). For I and N, \*\* $p$ <0.01, Student's two-tailed t-test. Data are means $\pm$ standard error of the mean. ABX, nonabsorbable antibiotics; LPS, lipopolysaccharides; ns, not significant; RTS, retrorsine; Veh, vehicle.

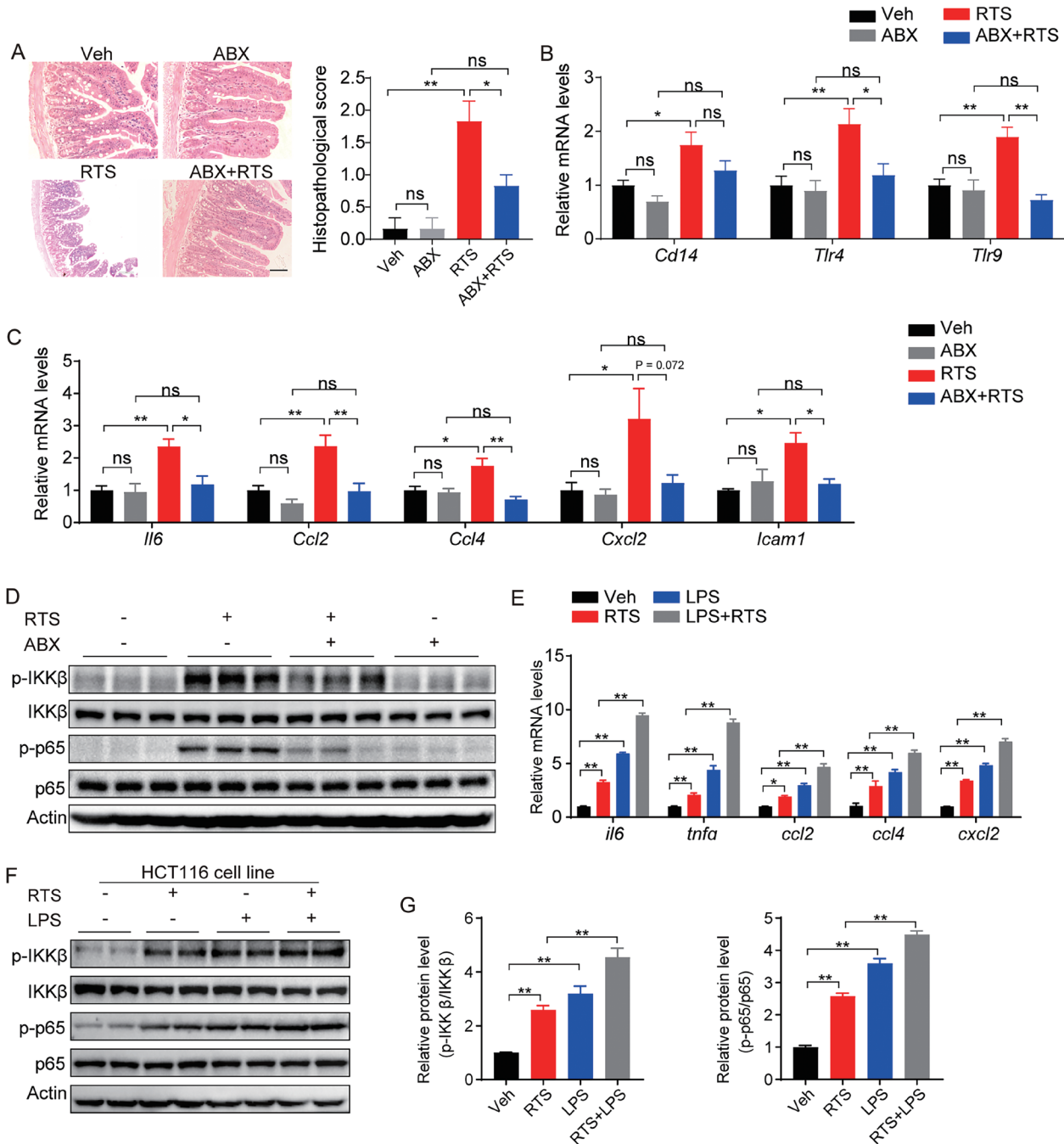


**Fig. 3. RTS cooperates with gut microbiota to induce intestinal inflammation.** (A) Representative ileal hematoxylin and eosin staining ( $n=6$  per group). Scale bar, 100  $\mu\text{m}$ . (B, C) mRNA expression of innate immune components (*Cd14*, *Tlr4*, *Tlr9*) and inflammatory cytokines (*Il6*, *ccl2*, *Ccl4*, *Cxcl2*, and *Icam1*) in the distal ileum of mice treated with RTS for 24 h with or without ABX pretreatment ( $n=6$  per group). (D) Protein expression of IKK $\beta$ , p-IKK $\beta$ , p65, and p-p65 in the distal ileum. GAPDH was the loading control ( $n=3$ ). (E) mRNA expression of proinflammatory factors (*Il6*, *Tnfa*, *Ccl2*, *Ccl4* and *Cxcl2*) in HCT116 cells ( $n=3$ ). (F) Protein expression of IKK $\beta$ , p-IKK $\beta$ , p65, and p-p65 in HCT116 cells. GAPDH was the loading control ( $n=3$ ). (G) Relative expression of IKK $\beta$ , p-IKK $\beta$ , p65, and p-p65 in HCT116 cells ( $n=3$ ). Veh, control group treated with vehicle; LPS group, HCT116 cells stimulated with LPS (5  $\mu\text{g}/\text{mL}$ ) for 24 h; RTS group, HCT116 cells stimulated with RTS (600  $\mu\text{M}$ ) for 24 h; RTS + LPS group included HCT116 cells costimulated with RTS (600  $\mu\text{M}$ ) and LPS (5  $\mu\text{g}/\text{mL}$ ) for 24 h. Data are means  $\pm$  standard error of the mean. \* $p < 0.05$ , \*\* $p < 0.01$ ; analysis of variance. ABX, nonabsorbable antibiotics; LPS, lipopolysaccharides; ns, not significant; RTS, retrorsine; Veh, vehicle.

**RTS and gut microbiota synergistically destroy the intestinal epithelial barrier in HSOS**

The destruction of the intestinal barrier is a prerequisite for

intestinal macromolecules to enter into intestinal lamina propria. We next detected epithelial tight junction markers, which sustain the function of the intestinal epithelial barrier. As it was shown, there was a sharp downregulation of the mRNA levels of tight junction molecules such as zonula oc-

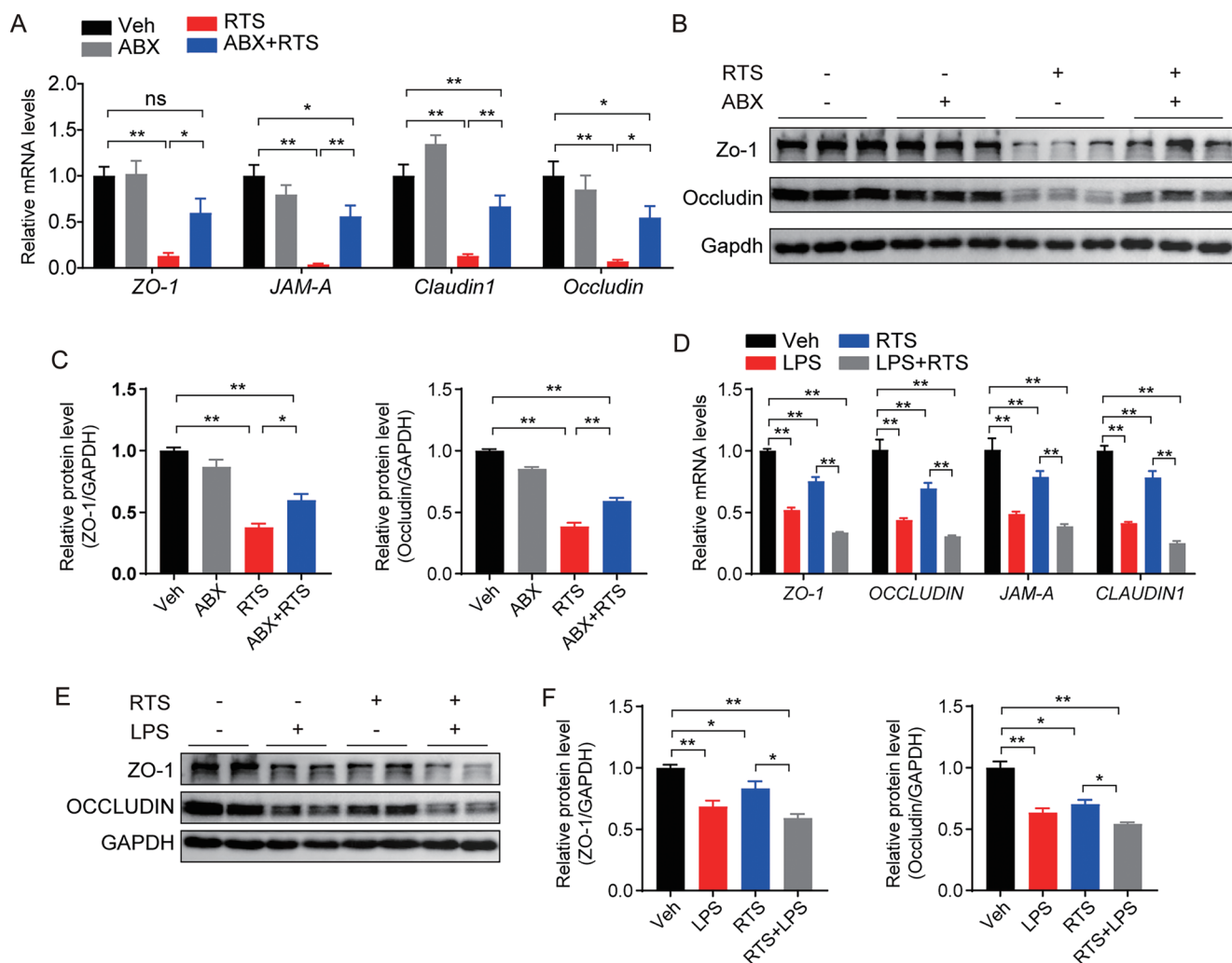


**Fig. 4. RTS and gut microbiota synergistically destroy the intestinal epithelial barrier in HSOS model mice.** (A) mRNA levels of ileal tight junction molecules ( $n=6$ ). (B) Protein levels and (C) Relative expression of ZO-1 and occludin in the distal ileum, GAPDH was the loading control ( $n=3$ ). (D) mRNA levels of ileum tight junction molecules in Caco2 cells ( $n=3$ ). (E) Protein levels and (F) Relative expression of ZO-1 and occludin in Caco2 cells, GAPDH was the loading control ( $n=3$ ). Data are means $\pm$ standard error of the mean. ns: no significance,  $*p<0.05$ ,  $**p<0.01$ ; analysis of variance. ABX, nonabsorbable antibiotics; LPS, lipopolysaccharides; ns, not significant; RTS, retrorsine; Veh, vehicle.

cludens 1 (*ZO-1*), occludin, junctional adhesion molecular A (*JAM-A*), and *Claudin1* in RTS mice compared with the vehicle-treated mice. ABX administration largely reversed the decrease in the expression of the mRNAs of the tight junction molecules in RTS-treated mice (Fig. 4A). Also, the expression of ZO-1 and occludin proteins was consistent with the gene expression (Fig. 4B, 4C), which suggests that RTS impaired the epithelial barrier. Subsequently, we performed *in vitro* experiments to further substantiate the disruption of RTS of the integrity of the intestinal epithelial barrier. Caco2 cells were stimulated with RTS (600  $\mu\text{mol/L}$ ) and LPS (10  $\mu\text{g/mL}$ ) for 24 h to mimic the intestinal micro-environment. We observed that RTS and LPS synergistically destroyed the intestinal epithelial barrier both at the gene and protein levels (Fig. 4D–F), indicating that RTS treatment indeed destroyed the integrity of cellular barriers that further aggravated by LPS. The results demonstrate that RTS administration caused intestinal epithelial barrier dysfunction that was inhibited by pretreatment ABX and indicates that gut flora participated in the RTS-elicited epithelial barrier disruption.

#### **RTS combines gut microbiota to increase vascular permeability to macromolecules in HSOS mice**

In addition to evaluating the integrity of the intestinal epithelial barrier, we investigated the interference of systematic translocation interception of bacteria or bacterial products by the GVB. Because disruption of the GVB permeability was indicated by leakage of 70 kD FITC-dextran (FD70) in the circulation, we looked for detectable FD70 macromolecules in the liver, spleen, and serum at 1 h after injection into a ligated ileal loop. After injection, the FITC fluorescence intensity in the liver was significantly augmented by RTS compared with vehicle, and the effect was reversed by ABX pretreatment (ABX+RTS, Fig. 5A). Similar scenarios were observed in the spleen (Fig. 5B) and the the serum (Fig. 5C). Furthermore, expression of plasmalemma vesicle-associated protein-1 (PV1), a regulator of vascular permeability, was significantly increased in the ileum of the RTS group compared with the vehicle or ABX+RTS (Fig. 5D). The results demonstrate that the GVB was impaired in RTS-induced HSOS, and decontami-

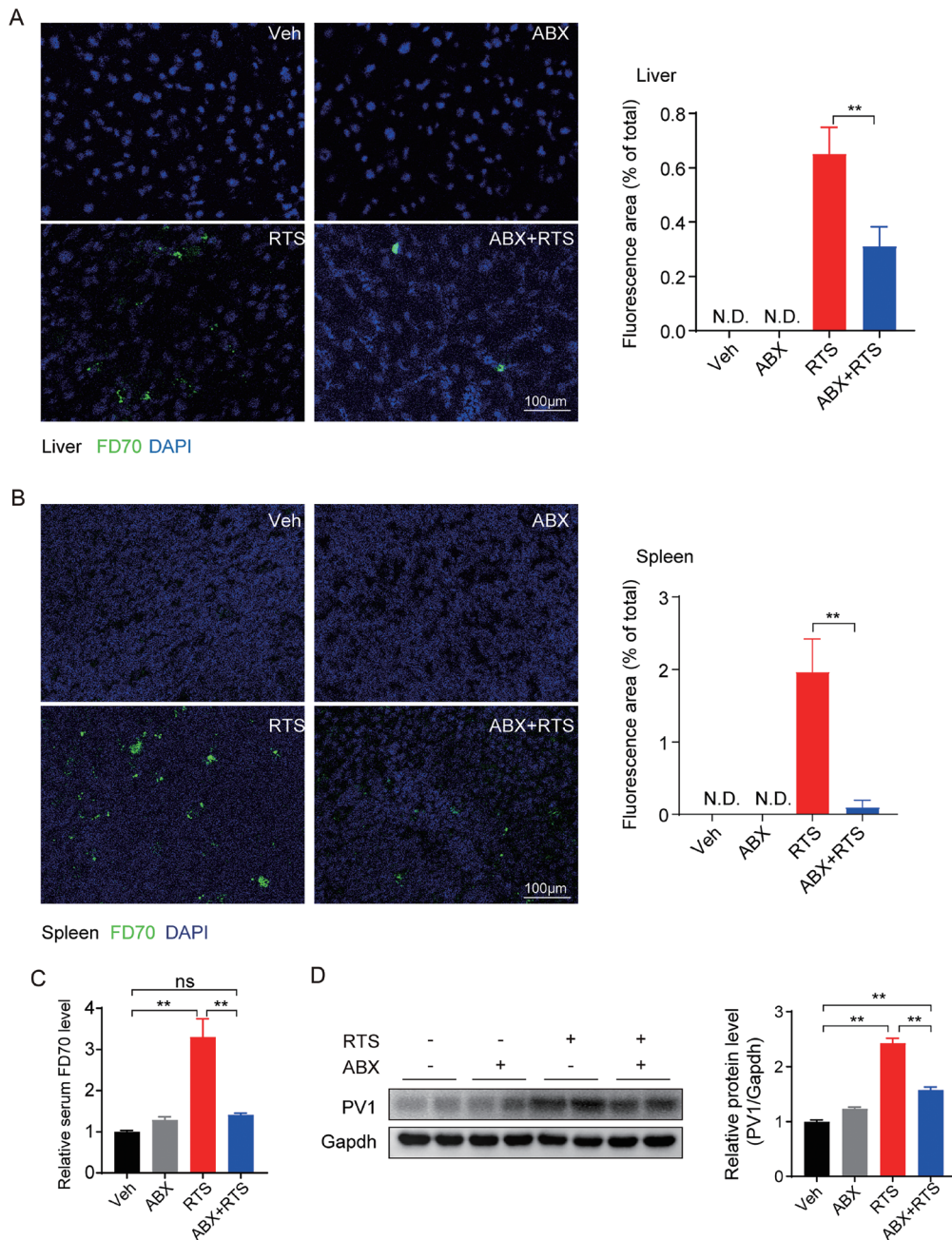


**Fig. 5. RTS combines with gut microbiota to increase vascular permeability to macromolecules in HSOS mice.** FD70 density (green) and the percentage of fluorescence area in (A) the liver and (B) spleen, and (C) relative serum FD70 levels 1 h after intestinal injection ( $n=5$  or  $6$ ). (D) Protein level (left) and Relative expression (right) of PV-1 in the distal ileum, GAPDH was the loading control ( $n=3$ ). Scale bar,  $50\ \mu\text{m}$ . Data are means $\pm$ standard error of the mean.  $**p<0.01$ ; analysis of variance. ABX, nonabsorbable antibiotics; FD70, 70 kD fluorescein isothiocyanate-dextran; LPS, lipopolysaccharides; PV1, plasmalemmal vesicle-associated protein-1; ND, not detectable; ns, no significance; RTS, retrorsine; Veh, vehicle.

nation of the microbiota with ABX reversed the compromise of the GVB, indicating that RTS-induced gut dysbiosis impaired the integrity of the GVB.

**Decontamination inhibits hepatic LPS-NF- $\kappa$ B pathway activation in RTS-induced HSOS**

Considering that LPS was significantly increased in portal

vein serum, we measured the concentration of the inflammatory cytokines in serum stimulated by LPS including IL6 and TNF- $\alpha$ . RTS significantly increased serum IL6 (Fig. 6A) and TNF- $\alpha$  (Fig. 6B) compared with the other study groups, and decontaminating the flora with ABX significantly attenuated the elevation of IL6 and TNF- $\alpha$  levels in HSOS mice. As LPS activates the NF- $\kappa$ B signaling pathway and subsequently regulates inflammation-related gene expression in liver, we investigated whether RTS alone or in collaboration with

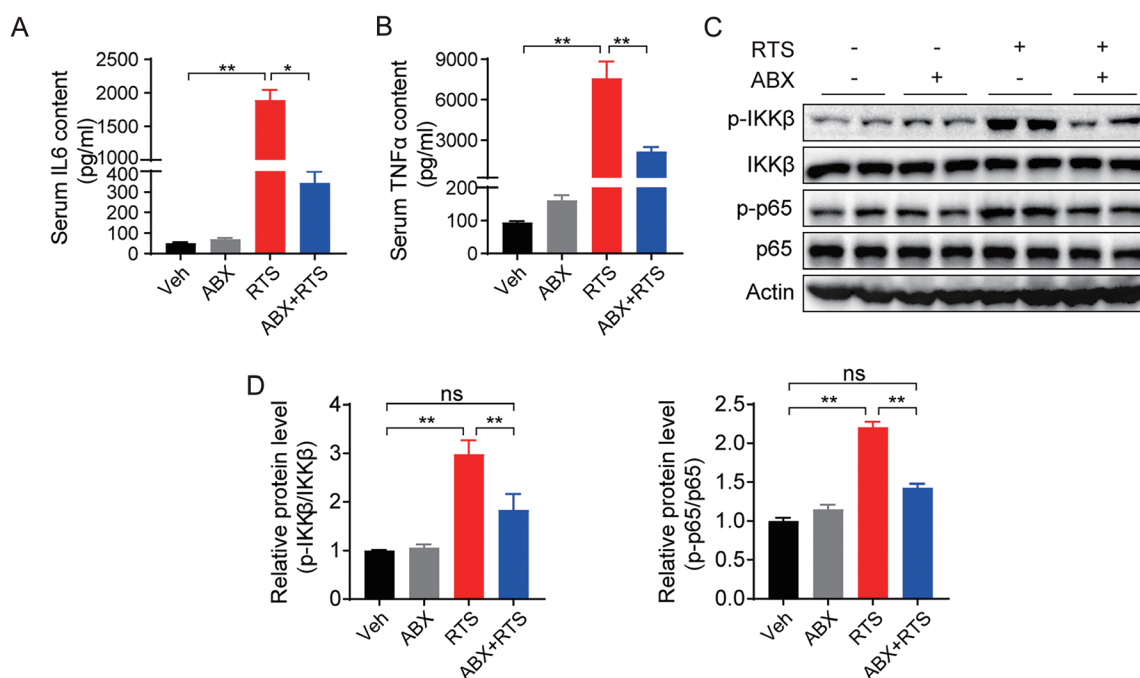


**Fig. 6. Decontamination inhibits hepatic LPS-NF-κB pathway activation in RTS-induced HSOS.** (A) Serum IL6 levels in mice ( $n=8$  per group). (B) Serum TNFα levels in mice ( $n=8$  per group). (C) Western blots and (D) relative expression of IKKβ, p-IKKβ, P65, and p-P65 protein in the liver. GAPDH was the loading control ( $n=3$  per group). Data are means±standard error of the mean. ns: no significance,  $*p<0.05$ ,  $**p<0.01$ ; analysis of variance. ABX, nonabsorbable antibiotics; RTS, retrorsine; Veh, vehicle.

gut microbiota increased NF-κB signaling pathway. As we have shown, RTS significantly enhanced the phosphorylation of hepatic IKKβ and p65, which reflect activation of the NF-κB signaling pathway. Similarly, preprocessing with ABX reversed the phosphorylation of IKKβ and p65 in liver (Fig. 6C). The difference in protein levels between the vehicle group and the RTS group was significant (Fig. 6D). Together, the findings demonstrate that intestinal decontamination significantly improved LPS-activated inflammation pathways in the livers of mice with RTS-induced HSOS, further confirming that gut microbiota promoted the progression of HSOS induced by RTS.

**LPS level was positively correlated with model for end-stage liver disease (MELD) score in patients with HSOS**

Having shown that RTS impaired the permeability of intestinal barrier and caused the translocation of enterotoxin into the portal vein, we also determined the serum LPS concentration in patients with HSOS attributed to exposure to the Chinese medicine Tusanqi, which contains Pas. Patients with HSOS are characterized by significant increases of GGT, ALP, Tbil, Dbil, creatinine, PT, and the INR as well as the reduction of albumin (Table 1). HSOS patients had slightly increased C-reactive protein, which was most likely related to Gram-negative bacterial infections. As shown in Figure 7A, compared with healthy control group, patients with HSOS had higher serum LPS levels, suggesting that enterotoxin translocation and a compromised intestinal barrier was involved in the pathogenesis of HSOS. We used MELD scores to access the severity of liver disease and evaluate the correlation with LPS concentration. To our surprise, the LPS level positively correlated with the MELD score in patients with HSOS (Fig.

7B), implying that serum LPS might predict the severity and dysbiosis of HSOS.

**Discussion**

HSOS is a life-threatening liver disease with very high mortality caused by severe liver failure and the absence of effective pharmacotherapies. A better understanding of the pathogenesis may help to prevent fatal outcomes of HSOS. Substantial evidence indicates that liver injury is closely related to the gut microbiota,<sup>24</sup> but most evidence was obtained in chronic liver diseases, such as nonalcoholic fatty liver disease.<sup>25</sup> The role of gut microbiota in PA-induced hepatotoxicity has not been well demonstrated. Therefore, it is indispensable to explore the relationship between gut microbiota and Pas-induced HSOS to improve prevention and treatment. Many studies have demonstrated that dysbiosis insults the intestinal barrier and increases intestinal inflammation.<sup>17,26</sup> The loss of integrity makes the gut epithelium more permissive to microbial LPS, trimethylamine (TMA), and other metabolites entering the circulation and contributing to liver inflammation.<sup>27</sup> In this study, we demonstrated that RTS modified the gut microbiota composition, resulting in elevated circulating LPS and that RTS cooperated with gut dysbiosis to intensify intestinal inflammation and destroy the intestinal epithelial barrier and GVB. Subsequently, the GVB disruption increased the permeability of intestinal macromolecules in RTS mice. Intestinal decontamination strongly inhibited the hepatic LPS-NF-κB pathway activation in RTS-induced HSOS. Importantly, clinical data indicated that the elevation of LPS in patients with HSOS was significantly associated with liver dysfunction, which further supports cooperation of RTS with gut microbiota and gut-derived bacterial LPS promotion of HSOS by disrupting the gut barrier.

**Table 1. Patient clinical characteristics**

	Normal	HSOS	p-value
Age (years)	51.67±6.46	60.17±3.31	0.209
Sex, male/female (n)	6/6	8/4	
ALT (U/L)	20.67±4.47	63.75±18.29	0.123
AST (U/L)	20±2.14	80.25±14.51	0.011
GGT (U/L)	20±4.71	199.83±50.96	0.026
ALP (U/L)	59.67±3.76	172.33±25.40	0.007
TBil (µmol/L)	13.5±2.59	70.16±17.19	0.036
DBil (µmol/L)	2.65±0.91	21.52±11.31	0.263
Total protein (g/L)	69.7±2.37	56.29±2.03	0.001
Albumin (g/L)	43.02±2.09	28.96±0.98	0.001
CRP (mg/L)	ND	14.07±2.95	
Creatinine (µmol/L)	59.4±3.03	82.19±8.55	0.086
PT (s)	12.97±0.27	17.09±0.67	0.001
INR	1±0.03	1.42±0.07	0.001

Data are means±standard error of the mean. ALP, alkaline phosphatase; ALT, alanine aminotransferase; AST, alanine aminotransferase; CRP, C reactive protein; DBil, direct bilirubin; GGT, gamma-glutamyl transpeptidase; INR, international normalized ratio, ND, not determined; PT, prothrombin time; TBil, total bilirubin.

The gut microbiota has been reported to contribute to various liver diseases,<sup>9,28,29</sup> but it remains unclear how changes in the intestinal microbiota influence HSOS. In this study, we observed that the abundance of Firmicutes was significantly decreased and the abundance of Bacteroidetes was increased in RTS-induced HSOS mice relative to the vehicle, reflecting nature of the shift in microbial composition.<sup>30</sup> The increased relative abundance of Gram-negative bacteria resulted in increased release of LPS in RTS-induced mice compared with vehicle mice. At the family level, the dominant Ruminococcaceae and Lachnospiraceae declined and Bacteroidaceae and Enterobacteriaceae were increased in the HSOS mice. Ruminococcaceae and Lachnospiraceae are butyrate-producing bacteria,<sup>31,32</sup> and butyrate has well-known anti-inflammatory properties. RTS administration may result in the intestinal microbiota shifting to inflammatory flora. In addition, many taxa frequently enriched in HSOS individuals, such as Enterobacteriaceae have pathogenic potential and Prevotellaceae are linked with inflam-

mation and the activation of gut dendritic cells.<sup>33,34</sup> At the genus level, we found the abundance of *Bacteroides* and *Escherichia* generating abundant LPS<sup>35</sup> was significantly increased in RTS-treated mice compared with the vehicle mice, which is consistent with the enhanced level of serum LPS. A recent study reported that increased hepatocyte LPS content occurred in parallel with increased serum LPS and was correlated with liver damage via the TLR4 signaling pathway.<sup>36</sup> LPS led to liver inflammation with upregulation of IL6 and TNF-α and activation of the pro-inflammatory NF-κB (IKKβ/p65) transcription factor complex which is in accord with previously reported evidence.<sup>37</sup> Furthermore, there is a report *Bacteroides* was a precipitating factor for thrombosis<sup>38</sup> and was significantly associated plasma TMA and/or TMAO levels,<sup>39</sup> implying that dysbiosis induced by RTS may be involved in the congestion of hepatic sinusoids, but that remains to be determined by the future studies. Taken together with prior studies demonstrating dysbiotic microbiota generate excess LPS and contribute to

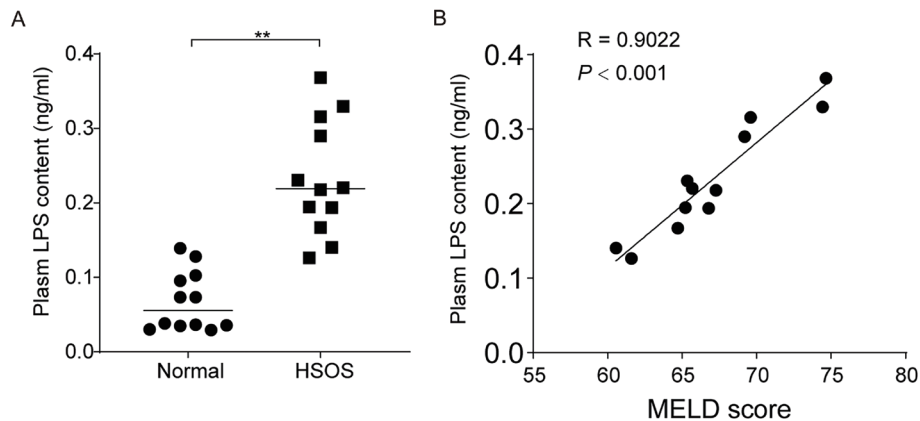


**Fig. 7. LPS level positively correlates with MELD score in patients with HSOS.** (A) Plasma LPS level of normal controls and HSOS patients (n=12 per group). Data are mean±standard error of the mean (two-tailed Student's t-test). (B) Correlation of plasma LPS level and MELD score in patients with HSOS (Spearman's rank correlation). \*\*p<0.01. MELD score calculated as (9.57 × log<sub>e</sub> creatinine mg/dL + 3.78 × log<sub>e</sub> bilirubin mg/dL + 11.20 × log<sub>e</sub> INR + 6.43). HSOS, hepatic sinusoidal obstruction syndrome; INR, international normalized ratio; MELD, model for end-stage liver disease.

inflammatory responses, our study adds to the data that the shifting of the gut bacterial composition increases LPS levels related to liver injury in RTS-induced HSOS mice. Modification of the gut microbiota may be a useful therapy for HSOS.

Dysbiosis and increased gut-derived bacterial LPS promote intestinal inflammation.<sup>40,41</sup> As shown, RTS administration caused low-grade intestinal inflammation and activated the NF- $\kappa$ B pathway. The effects of RTS were reversed by ABX pretreatment. We performed *in vitro* cell experiments to substantiate the results. We found that RTS and LPS synergistically generated higher expression of inflammation-related genes and NF- $\kappa$ B pathway activation. Our results confirmed that RTS-induced dysbiosis could intensify RTS-induced intestinal inflammation. Taken together, the data imply that RTS collaborated with the gut microbiota to drive activation of intestinal inflammation via the LPS-activated NF- $\kappa$ B signaling pathway, which represents an important contribution to the pathogenesis of HSOS.

There is evidence that the damage to the intestinal epithelial and vascular barriers driven by dysbiosis has a key role in controlling the translocation of microbial components and metabolites into the circulation.<sup>16,42</sup> Although RTS administration remarkably altered the composition of the microbial community in HSOS mice, gut barrier permeability it remains to be examined in mice with RTS-induced HSOS. Assays of the expression of intestinal epithelial tight junction proteins and mRNAs revealed a significant loss of tight junction proteins, such as ZO-1 and occludin in mice with RTS-induced HSOS, which was reversed by ABX pretreatment, suggesting that the microbiota had a negative effect by disrupting the epithelial barrier. However, whether bacterial components can access the liver may be determined by the GVB.<sup>42</sup> A regulator of vascular permeability, PV1, was used to detect changes in the GVB,<sup>42,43</sup> and the detection of increased endothelial PV-1 expression in RTS-treated mice implies disruption of the GVB in RTS-induced HSOS. In addition, as macromolecules as large as 70 kDa are not present in circulation unless the GVB is impaired, so we used FD70 to estimate GVB permeability. Consistent with the PV1 level, higher fluorescence intensity of FD70 was measured in the liver, spleen, and serum in RTS mice relative to vehicle and ABX pretreatment groups. It further substantiated GVB disruption during HSOS. Intriguingly, gut bacterial decontamination improved the compromise of GVB in HSOS, indicating that the intestinal flora mediated the GVB disruption induced by RTS. Collectively, insult to intestinal barriers facilitated translocation of bacterial endotoxin into the liver and the subsequent induction of inflammatory responses by the LPS-activated NF- $\kappa$ B signaling pathway to further promote HSOS progression. There is a lack of effective therapeutics, and our study indicates that antibiotics may be a potential treatment option that needs confirmation by clinical trials.

In conclusion, this study demonstrated that RTS cooperated with gut dysbiosis to result in intestinal inflammation and gut barrier compromise in HSOS mice. Our findings provide the first solid evidence for the involvement of gut microbiota in the development of HSOS induced by RTS and also describes a novel mechanism for the progression of RTS-induced HSOS. Modulating the gut microbiota, protecting the intestinal barrier, and suppressing intestinal inflammation with prebiotics or antibiotics has the potential to become a pharmacologic intervention for HSOS.

## Acknowledgments

We thank Yixin Zhu for help in polishing the language and grammar.

## Funding

This study was supported by the National Natural Science Foundation of China (No. 81974078, 81570530, 81370550 to LY, No. 8190034336 to WW) and Natural Science Foundation of Hubei Province (No. 2019ACA133 to LY)

## Conflict of interest

The authors have no conflict of interests related to this publication.

## Author contributions

Experiments, analysis, interpretation of data and manuscript drafting (LX, LH, HC, LC), acquisition of data (JY, XY, FD, QZ), critical revision of the manuscript for important intellectual content (WW, PC, XH. LY), material support (YS), and study supervision, study concept and design (LY).

## Data sharing statement

The datasets used in the current study are available from the corresponding author on reasonable request.

## References

- [1] Mahadeo KM, Bajwa R, Abdel-Azim H, Lehmann LE, Duncan C, Zantek N, *et al*. Diagnosis, grading, and treatment recommendations for children, adolescents, and young adults with sinusoidal obstructive syndrome: an international expert position statement. *Lancet Haematol* 2020;7(1):e61–e72. doi:10.1016/s2352-3026(19)30201-7, PMID:31818728.
- [2] Lin G, Wang JY, Li N, Li M, Gao H, Ji Y, *et al*. Hepatic sinusoidal obstruction syndrome associated with consumption of *Gynura segetum*. *J Hepatol* 2011;54(4):666–673. doi:10.1016/j.jhep.2010.07.031, PMID:21146894.
- [3] Moreira R, Pereira DM, Valentão P, Andrade PB. Pyrrolizidine Alkaloids: Chemistry, Pharmacology, Toxicology and Food Safety. *Int J Mol Sci* 2018;19(6):1668. doi:10.3390/ijms19061668, PMID:29874826.
- [4] Robertson J, Stevens K. Pyrrolizidine alkaloids: occurrence, biology, and chemical synthesis. *Nat Prod Rep* 2017;34(1):62–89. doi:10.1039/c5np00076a, PMID:27782262.
- [5] Yang X, Li W, Sun Y, Guo X, Huang W, Peng Y, *et al*. Comparative Study of Hepatotoxicity of Pyrrolizidine Alkaloids Retrorsine and Monocrotaline. *Chem Res Toxicol* 2017;30(2):532–539. doi:10.1021/acs.chemrestox.6b00260, PMID:28095673.
- [6] Wang JB, Zhu Y, Bai ZF, Wang FS, Li XH, Xiao XH, *et al*. Guidelines for the Diagnosis and Management of Herb-Induced Liver Injury. *Chin J Integr Med* 2018;24(9):696–706. doi:10.1007/s11655-018-3000-8, PMID:29542018.
- [7] Wiest R, Albillos A, Trauner M, Bajaj JS, Jalan R. Targeting the gut-liver axis in liver disease. *J Hepatol* 2017;67(5):1084–1103. doi:10.1016/j.jhep.2017.05.007, PMID:28526488.
- [8] Albillos A, de Gottardi A, Rescigno M. The gut-liver axis in liver disease: Pathophysiological basis for therapy. *J Hepatol* 2020;72(3):558–577. doi:10.1016/j.jhep.2019.10.003, PMID:31622696.
- [9] Gong S, Lan T, Zeng L, Luo H, Yang X, Li N, *et al*. Gut microbiota mediates diurnal variation of acetaminophen induced acute liver injury in mice. *J Hepatol* 2018;69(1):51–59. doi:10.1016/j.jhep.2018.02.024, PMID:29524531.
- [10] Fouts DE, Torralba M, Nelson KE, Brenner DA, Schnabl B. Bacterial translocation and changes in the intestinal microbiome in mouse models of liver disease. *J Hepatol* 2012;56(6):1283–1292. doi:10.1016/j.jhep.2012.01.019, PMID:22326468.
- [11] Wiest R, Lawson M, Geuking M. Pathological bacterial translocation in liver cirrhosis. *J Hepatol* 2014;60(1):197–209. doi:10.1016/j.jhep.2013.07.044, PMID:23993913.
- [12] Wahlström A, Sayin SI, Marschall H-U, Bäckhed F. Intestinal Crosstalk between Bile Acids and Microbiota and Its Impact on Host Metabolism. *Cell metabolism* 2016;24(1):41–50. doi:10.1016/j.cmet.2016.05.005, PMID:27320064.
- [13] Ma C, Han M, Heinrich B, Fu Q, Zhang Q, Sandhu M, *et al*. Gut microbiome-mediated bile acid metabolism regulates liver cancer via NKT cells. *Science* 2018;360(6391):eaan5931. doi:10.1126/science.aan5931, PMID:29798856.
- [14] Spadoni I, Fornasa G, Rescigno M. Organ-specific protection mediated by cooperation between vascular and epithelial barriers. *Nature reviews. Immunology* 2017;17(12):761–773. doi:10.1038/nri.2017.100, PMID:28869253.

- [15] Peterson LW, Artis D. Intestinal epithelial cells: regulators of barrier function and immune homeostasis. *Nat Rev Immunol* 2014;14(3):141–153. doi:10.1038/nri3608, PMID:24566914.
- [16] Mouries J, Brescia P, Silvestri A, Spadoni I, Sorribas M, Wiest R, *et al*. Microbiota-driven gut vascular barrier disruption is a prerequisite for non-alcoholic steatohepatitis development. *J Hepatol* 2019;71(6):1216–1228. doi:10.1016/j.jhep.2019.08.005, PMID:31419514.
- [17] Yu LC, Wang JT, Wei SC, Ni YH. Host-microbial interactions and regulation of intestinal epithelial barrier function: From physiology to pathology. *World J Gastrointest Pathophysiol* 2012;3(1):27–43. doi:10.4291/wjgp.v3.i1.27, PMID:22368784.
- [18] Chen M, Li L, Zhong D, Shen S, Zheng J, Chen X. 9-Glutathionyl-6,7-dihydro-1-hydroxymethyl-5H-pyrrolizine Is the Major Pyrrolic Glutathione Conjugate of Retronecine-Type Pyrrolizidine Alkaloids in Liver Microsomes and in Rats. *Chem Res Toxicol* 2016;29(2):180–189. doi:10.1021/acs.chemrestox.5b00427, PMID:26761523.
- [19] Gordon GJ, Coleman WB, Grisham JW. Bax-mediated apoptosis in the livers of rats after partial hepatectomy in the retrorsine model of hepatocellular injury. *Hepatology* 2000;32(2):312–320. doi:10.1053/jhep.2000.9144, PMID:10915738.
- [20] Edgar RC. UPARSE: highly accurate OTU sequences from microbial amplicon reads. *Nat Methods* 2013;10(10):996–998. doi:10.1038/nmeth.2604, PMID:23955772.
- [21] Caporaso JG, Kuczynski J, Stombaugh J, Bittinger K, Bushman FD, Costello EK, *et al*. QIIME allows analysis of high-throughput community sequencing data. *Nat Methods* 2010;7(5):335–336. doi:10.1038/nmeth.f.303, PMID:20383131.
- [22] Hahn A, Sanyal A, Perez GF, Colberg-Poley AM, Campos J, Rose MC, *et al*. Different next generation sequencing platforms produce different microbial profiles and diversity in cystic fibrosis sputum. *J Microbiol Methods* 2016;130:95–99. doi:10.1016/j.mimet.2016.09.002, PMID:27609714.
- [23] Segata N, Izard J, Waldron L, Gevers D, Miropolsky L, Garrett WS, *et al*. Metagenomic biomarker discovery and explanation. *Genome Biol* 2011;12(6):R60. doi:10.1186/gb-2011-12-6-r60, PMID:21702898.
- [24] Wang R, Tang R, Li B, Ma X, Schnabl B, Tilg H. Gut microbiome, liver immunology, and liver diseases. *Cell Mol Immunol* 2021;18(1):4–17. doi:10.1038/s41423-020-00592-6, PMID:33318628.
- [25] Boursier J, Mueller O, Barret M, Machado M, Fizanne L, Araujo-Perez F, *et al*. The severity of nonalcoholic fatty liver disease is associated with gut dysbiosis and shift in the metabolic function of the gut microbiota. *Hepatology* 2016;63(3):764–775. doi:10.1002/hep.28356, PMID:26600078.
- [26] Mouries J, Brescia P, Silvestri A, Spadoni I, Sorribas M, Wiest R, *et al*. Microbiota-driven gut vascular barrier disruption is a prerequisite for non-alcoholic steatohepatitis development. *J Hepatol* 2019;71(6):1216–1228. doi:10.1016/j.jhep.2019.08.005, PMID:31419514.
- [27] Dabke K, Hendrick G, Devkota S. The gut microbiome and metabolic syndrome. *J Clin Invest* 2019;129(10):4050–4057. doi:10.1172/jci129194, PMID:31573550.
- [28] Leung C, Rivera L, Furness JB, Angus PW. The role of the gut microbiota in NAFLD. *Nat Rev Gastroenterol Hepatol* 2016;13(7):412–25. doi:10.1038/nrgastro.2016.85, PMID:27273168.
- [29] Llopis M, Cassard AM, Wrzosek L, Boschat L, Bruneau A, Ferrere G, *et al*. Intestinal microbiota contributes to individual susceptibility to alcoholic liver disease. *Gut* 2016;65(5):830–839. doi:10.1136/gutjnl-2015-310585, PMID:26642859.
- [30] De Filippo C, Cavalieri D, Di Paola M, Ramazzotti M, Poullet JB, Massart S, *et al*. Impact of diet in shaping gut microbiota revealed by a comparative study in children from Europe and rural Africa. *Proc Natl Acad Sci U S A* 2010;107(33):14691. doi:10.1073/pnas.1005963107, PMID:20679230.
- [31] Clark A, Sallé G, Ballan V, Reigner F, Meynadier A, Cortet J, *et al*. Strongyle Infection and Gut Microbiota: Profiling of Resistant and Susceptible Horses Over a Grazing Season. *Front Physiol* 2018;9:272. doi:10.3389/fphys.2018.00272, PMID:29618989.
- [32] Flint HJ, Bayer EA, Rincon MT, Lamed R, White BA. Polysaccharide utilization by gut bacteria: potential for new insights from genomic analysis. *Nat Rev Microbiol* 2008;6(2):121–131. doi:10.1038/nrmicro1817, PMID:18180751.
- [33] Scher JU, Sczesnak A, Longman RS, Segata N, Ubeda C, Bielski C, *et al*. Expansion of intestinal *Prevotella copri* correlates with enhanced susceptibility to arthritis. *eLife* 2013;2:e01202. doi:10.7554/eLife.01202, PMID:24192039.
- [34] Dillon SM, Lee EJ, Kotter CV, Austin GL, Gianella S, Siewe B, *et al*. Gut dendritic cell activation links an altered colonic microbiome to mucosal and systemic T-cell activation in untreated HIV-1 infection. *Mucosal Immunol* 2016;9(1):24–37. doi:10.1038/mi.2015.33, PMID:25921339.
- [35] Vatanen T, Kostic AD, d’Hennezel E, Siljander H, Franzosa EA, Yassour M, *et al*. Variation in Microbiome LPS Immunogenicity Contributes to Autoimmunity in Humans. *Cell* 2016;165(4):842–853. doi:10.1016/j.cell.2016.04.007, PMID:27133167.
- [36] Carpino G, Del Ben M, Pastori D, Carnevale R, Baratta F, Overi D, *et al*. Increased liver localization of lipopolysaccharides in human and experimental non-alcoholic fatty liver disease. *Hepatology* 2020;72(2):470–485. doi:10.1002/hep.31056, PMID:31808577.
- [37] Xie QW, Kashiwabara Y, Nathan C. Role of transcription factor NF-kappa B/Rel in induction of nitric oxide synthase. *J Biol Chem* 1994;269(7):4705–4708. PMID:7508926.
- [38] Denninger MH, Chait Y, Casadevall N, Hillaire S, Guillin MC, Bezaud A, *et al*. Cause of portal or hepatic venous thrombosis in adults: the role of multiple concurrent factors. *Hepatology* 2000;31(3):587–591. doi:10.1002/hep.510310307, PMID:10706547.
- [39] Chen ML, Yi L, Zhang Y, Zhou X, Ran L, Yang J, *et al*. Resveratrol Attenuates Trimethylamine-N-Oxide (TMAO)-Induced Atherosclerosis by Regulating TMAO Synthesis and Bile Acid Metabolism via Remodeling of the Gut Microbiota. *mBio* 2016;7(2):e02210–15. doi:10.1128/mBio.02210-15, PMID:27048804.
- [40] Chen P, Stärkel P, Turner JR, Ho SB, Schnabl B. Dysbiosis-induced intestinal inflammation activates tumor necrosis factor receptor I and mediates alcoholic liver disease in mice. *Hepatology* 2015;61(3):883–894. doi:10.1002/hep.27489, PMID:25251280.
- [41] Banerjee S, Sindberg G, Wang F, Meng J, Sharma U, Zhang L, *et al*. Opioid-induced gut microbial disruption and bile dysregulation leads to gut barrier compromise and sustained systemic inflammation. *Mucosal Immunol* 2016;9(6):1418–1428. doi:10.1038/mi.2016.9, PMID:26906406.
- [42] Spadoni I, Zagato E, Bertocchi A, Paolinelli R, Hot E, Di Sabatino A, *et al*. A gut-vascular barrier controls the systemic dissemination of bacteria. *Science* 2015;350(6262):830–834. doi:10.1126/science.aad0135, PMID:26564856.
- [43] Spadoni I, Fornasa G, Rescigno M. Organ-specific protection mediated by cooperation between vascular and epithelial barriers. *Nat Rev Immunol* 2017;17(12):761–773. doi:10.1038/nri.2017.100, PMID:28869253.